

Astrometrically Registered Simultaneous Observations of the 22 GHz H₂O and the 43GHz SiO masers towards R Leonis Minoris using KVN and Source/Frequency Phase Referencing

Richard DODSON^{1,2}, María J. RIOJA^{1,2,3}, Tae-Hyun JUNG¹, Bong-Won Sohn¹, Do-Young Byun¹, Se-Hyung Cho¹, Sang-Sung Lee¹, Jongsoo Kim¹, Kee-Tae Kim¹, Chung-Sik Oh¹, Seog-Tae Han¹, Do-Heung Je¹, Moon-Hee Chung¹, Seog-Oh Wi¹, Jiman Kang¹, Jung-Won Lee¹, Hyunsoo Chung¹, Hyo-Ryoung Kim¹, Hyun-Goo Kim¹, Chang-Hoon Lee¹, Duk-Gyoo Roh¹, Se-Jin Oh¹, Jae-Hwan Yeom¹, Min-Gyu Song¹, Yong-Woo Kang¹

¹ *Korea Astronomy and Space Science Institute, Daedeokdae-ro 776, Yuseong-gu, Daejeon 305-348, Korea*

² *International Centre for Radio Astronomy Research, M468, The University of Western Australia, 35 Stirling Hwy, Crawley, Western Australia, 6009*

³ *Observatorio Astronómico Nacional (IGN), Alfonso XII, 3 y 5, 28014 Madrid, Spain*

rdodson@kasi.re.kr

ABSTRACT

Oxygen-rich Asymptotic Giant Branch (AGB) stars can be intense emitters of SiO ($v=1$ and 2 , $J=1\rightarrow0$) and H₂O maser lines at 43 and 22 GHz, respectively. VLBI observations of the maser emission provide a unique tool to probe the innermost layers of the circumstellar envelopes in AGB stars. Nevertheless, the difficulties in achieving astrometrically aligned H₂O and $v=1$ and $v=2$ SiO maser maps have traditionally limited the physical constraints that can be placed on the SiO maser pumping mechanism. We present phase referenced simultaneous spectral-line VLBI images for the SiO $v=1$ and $v=2$, $J=1\rightarrow0$, and H₂O maser emission around the AGB star RLMi, obtained from the Korean VLBI Network (KVN). The simultaneous multi-channel receivers of the KVN offer great possibilities for astrometry in the frequency domain. With this facility we have produced images with bona-fide absolute astrometric registration between high frequency maser transitions of different species to provide the positions of the H₂O maser emission, and the centre of the SiO maser emission, and hence reducing the uncertainty in the proper motion for RLMi by an order of magnitude over that from Hipparcos. This is the first successful demonstration of source frequency phase referencing for mm-VLBI spectral-line observations and also where the ratio between the frequencies is not an integer.

Subject headings: Astrometry – techniques: interferometric – Masers (H₂O SiO)
 – Stars: AGB and post-AGB – Stars: individual (R LMi)

1. Introduction

O-rich Asymptotic Giant Branch (AGB) stars can be intense emitters of SiO and H₂O maser lines. There are many molecular lines which arise in AGB stars (Elitzur 1992), in particular those of SiO (for example Gray et al. (1999)) and H₂O (for example Benson & Little-Marenin (1996)). The most commonly studied are the 43-GHz SiO lines ($v=1$ and 2 , $J=1\rightarrow0$) and 22-GHz H₂O, ($J_{K-,K+}=6_{1,6}-5_{2,3}$). Simultaneous frequency single dish monitoring of these lines, along with others, are an active research effort at the KVN, e.g. Kim et al. (2010). SiO masers have very high excitation levels and so appear at a distance of a few stellar radii, $\sim 10^{14}$ cm, resulting in a more or less circular structure. H₂O emission is found further from the star, $\sim 10^{15}$ cm, with less well defined structures. A combined study of both masers can therefore produce a very accurate description of the structure and kinetics of these inner layers. In the inner-most regions of circumstellar shells, from which the whole circumstellar envelope will be formed, the dust grains are still growing and the gas has not yet attained its final expansion velocity, since expansion is supposed to be powered by radiation pressure onto the grains. The dynamics in the SiO emitting region is dominated by pulsation, which propagates from the photosphere via shocks, and by the first stages of outwards acceleration (Bowen 1988; Humphreys 2002; Gray et al. 2009). The H₂O emission, on the other hand, occurs where the acceleration process is almost completed. Their combined study therefore provides a powerful tool for the understanding the mass loss and the envelope formation processes in AGB stars.

To understand these mass loss processes we need to derive the underlying physical conditions from the observations of the maser emission. The theory for H₂O maser production is understood to be due to collisions with hydrogen (Cooke & Elitzur 1985), however the theory of the SiO maser excitation is the weakest link in the logical chain. For the SiO molecule there are currently two models, one based on radiative pumping (Bujarrabal 1994) from the NIR emission of the central star, the other on collisional pumping (Elitzur 1980; Humphreys et al. 2000) via the shock wave driven by stellar pulsation. If the latter is the correct model the prediction is that there would be no or little separation between the $v=1$ and $v=2$ SiO emission regions, whereas for the former the prediction is that there would be such a separation. Therefore the relative distribution of the spots at both the $v=1$ and $v=2$ SiO transitions is important to discriminate between the different pumping mechanisms. Existing multi-transitional maps (Desmurs et al. 2000; Yi et al. 2005; Boboltz & Wittkowski

2005; Soria-Ruiz et al. 2004, 2005, 2007; Rioja et al. 2008; Cotton et al. 2004, 2006, 2008; Cotton et al. 2009a,b, 2010a,b, 2011; Richter et al. 2013; Choi et al. 2008; Kamohara et al. 2010) suggest that the spots of these lines are generated in close proximity. One school of thought, however, reports that these emissions tend to be separated by about an AU (a mas at typical distances) or that the typical radius for the SiO transitions are different, thereby favouring the radiative pumping model; the other finds the emission coincident, thereby favouring the collision pumping model. However in the majority of cases the basis for these conclusions is either the assumption of a common origin for the centres of the SiO maser emissions or from alignment performed on cross correlation of the images. Neither method provides *bona-fide* astrometry. Only Rioja et al. (2008); Choi et al. (2008) and Kamohara et al. (2010) provide robust bona-fide astrometric registration between the SiO transitions, all from VERA observations. In Rioja et al. (2008) we observed R LMi and found only one site out of 17 spots produced overlapping $v=1$ and $v=2$ emission. Kamohara et al. (2010) and Choi et al. (2008) astrometrically observed R Aquilae and VY CMa respectively, also with VERA observations. Whilst Choi et al. (2008) had astrometrical information no comparison between the transitions was made. Kamohara et al. (2010) showed that only a few percent of the spots showed overlap between the $v=1$ and $v=2$ emission. Of the other observations only Boboltz & Wittkowski (2005) and Yi et al. (2005) attempted astrometry but these had narrow limited bandwidth coverage limiting the delay (and thus positional) accuracy or had a poor absolute coordinate position limiting the final relative positional accuracy.

In general the stellar positions are quite accurately measured for many AGB stars, with data from the Hipparcos satellite (Perryman et al. 1997) providing typical precision of 1 mas and it is expected that GAIA (Perryman et al. 2001) will provide precisions two orders of magnitude higher. It is therefore the VLBI studies of the SiO and H₂O maser spot distributions which are lacking accurate astrometric information in their relative and absolute coordinates of the maps of the different lines. Given the difficulties in providing these measurements with the existing facilities we have been investigating new astrometric methods.

The innovative multi-channel receiver (Han et al. 2008) of the Korean VLBI Network (KVN) (Lee et al. 2014) is designed to allow the transfer of the calibration solutions derived from the measurements on one frequency band (or ‘channel’ in their nomenclature) to the data from another frequency band. This provides the ideal design for experiments which benefit from simultaneous observations at different frequencies or spectral transitions. The KVN backend, combined with the Source Frequency Phase Referencing (SFPR) technique (Dodson & Rioja 2009; Rioja & Dodson 2011; Rioja et al. 2011), allows astrometrical observations even at the highest frequencies. We know of no demonstrated upper limit and it

would be expected to work as long as the tropospheric contributions were non-dispersive. Tests are on-going with ALMA (Fomalont 2014) at frequencies as high as 350 GHz, and so far have been successful. In Rioja et al. (2014) we make a detailed comparison between the KVN and the VLBA for continuum sources. The frequencies of spectral line emission do not necessarily fall on integer ratios and in this paper we focus only on the additional considerations and steps required for the analytical method in this case. Future publications with multiple epochs of data will be more suitable to explore the physical interpretation of the observations.

We present here the results from simultaneous KVN observations of SiO and H₂O maser emission in RLMi, and the first ever bona-fide absolute astrometric alignment between H₂O and ($v=1$ and $v=2$, $J=1\rightarrow0$) SiO maser emission derived from the SFPR astrometric analysis. RLMi is an O-rich Mira-type variable, with a pulsation period of about 373 days (Pardo et al. 2004) and a spectral type ranging between M6.5, at the optical maximum, and M9.0, at the minimum (Keenan et al. 1974). Its distance is assumed to be ~ 417 pc (Pickle & Depagne 2010), derived from the well-known period-luminosity relation (Whitelock et al. 2008). RLMi is a well known emitter in H₂O and SiO lines. In particular it was accurately monitored by Pardo et al. (2004), who found the periodic variation in radio flux in-phase with the IR cycle, typical of Mira-type stars.

In our previous publications (e.g. Rioja & Dodson (2011)) we strongly suggested that SFPR required an integer frequency ratio between the calibrating and the target frequencies. This is not always possible, particularly for spectral sources, where the line rest frequency sets the target frequencies. This effectively limited the spectral line science targets to be SiO masers, as the rotational emission modes for this molecule have almost exact integer frequency ratios. Here however we successfully phase referenced the SiO maser emission with measurements on H₂O maser emission, where the frequency ratio is around 1.9. This small offset from integer had been found to be sufficient to prevent success in previous attempts to achieve astrometry (Dodson & Rioja 2011). These early attempts failed because the calibration chain for the astrometric observations were insufficiently rigorous, as will be explained in the following sections.

The contents of the paper are organised as follows. The observational setup is described in Sect. 2. In Sect.3 we describe the special data reduction strategy used to preserve the relative astrometry between the maser transitions. In Sect.4 we briefly present the first astrometrically aligned maps and in Sect.5 we discuss the implications of this new method for the field.

2. Observations

We carried out simultaneous dual-frequency observations in early test time with the KVN (2011, March 4th) using all three antennas at Yonsei, Ulsan and Tamna. We recorded 8 narrow bands (intermediate-frequency bands, or IFs) of Left Hand Circular (LHC) 16MHz bandwidth from the 22GHz system and the same from the 43GHz system. The IFs were set as widely separated and as randomly distributed as possible across the available system bandwidth of 500MHz at each band, whilst including the target transitions, in order to suppress the delay sidelobes. At 22GHz the IFs were with lower band edges at 21.810, 21.826, 21.858, 21.922, 22.050, 22.114, 22.162, 22.226 GHz. This places the H_2O emission close to the centre of IF 8. For the 43GHz system we had IFs with lower band edges at 42.810, 42.826, 42.858, 42.922, 43.050, 43.114, 43.162, 43.226 GHz, with the $v=2$ SiO maser in IF 1 and $v=1$ SiO maser in IF 6. This distribution ensured that the first delay sidelobe, at $\sim 16\mu\text{sec}$, was less than 70% of the main peak.

We alternated observations between the target R LMi and the bright continuum fringe-finder and calibrator source, 4C39.25 (J0927+3902), with 2 minute scans on each. The angular separation between these two sources is 5.9° on the sky. The correlation was done with the DiFX correlator (Deller et al. 2011) with 1 second averaging and a spectral resolution of 1024 channels per IF, yielding maximum velocity resolutions of 0.1 km s^{-1} and 0.2 km s^{-1} for the line observations at 43 and 22 GHz, respectively, when using no spectral smoothing.

3. Data reduction for Source Frequency Phase Referencing Analysis

3.1. Basis of the Source Frequency Phase Referencing method

The full details of SFPR are provided in two VLBA memos (Dodson & Rioja 2009; Rioja & Dodson 2009) and in two journal papers (Rioja & Dodson 2011; Rioja et al. 2011). The method is generally applicable, but has particular relevance in cases where the frequency is so high that conventional phase referencing (PR) can not, or struggles to, succeed. In PR the antennas nod rapidly between a calibrator (assumed to be achromatic with no core-shift of its own, in both PR and SFPR) and the target (Alef 1988; Beasley & Conway 1995). For frequencies above 22GHz the coherence time becomes so short that it becomes increasingly difficult to slew from one source to the other and back within this period. Additionally the number of calibrators strong enough to be detected, yet within the same tropospheric ‘patch’ as the target, rapidly approaches zero. SFPR avoids this limit by observing at multiple frequencies and assuming that the atmosphere is dominated by non-dispersive contributions.

At mm-wavelengths this is certainly the case as the troposphere is the limiting source of error, and the troposphere is non-dispersive. By self-calibrating on the observations of the target source at the low (reference) frequency and applying those solutions to the higher frequency data we correct for the dominant non-dispersive terms. We call the resultant calibrated high frequency dataset “Frequency Phase Transferred” (*hereafter* FPT), or *troposphere-free*, target dataset. However the remaining dispersive errors prevent the recovery of the position of the target source, using a Fourier inversion, at this stage. The residual dispersive contributions arising from the ionospheric propagation and other effects need to be removed using the alternating observations of the second source. This source can be visited less frequently and can lie significantly further from the target than in conventional PR, as the residual terms these observations correct for are much weaker and vary much more slowly than the dominant tropospheric and other non-dispersive effects. After this second calibration step the resultant SFPR-calibrated data-sets can be Fourier inverted to provide the astrometrically registered target image between the two observing frequencies.

As stated the first step does not provide astrometry-ready data, as shown in Figure 1. Following equation 2 in Rioja & Dodson (2011), the FPT dataset has residual phases ϕ^{FPT} , that can be expressed as the sum of the contributions:

$$\begin{aligned} \phi^{\text{FPT}} = & \phi^{\text{high}} - R \cdot \phi_{\text{self-cal}}^{\text{low}} = \phi_{\text{str}}^{\text{high}} \\ & + (\phi_{\text{geo}}^{\text{high}} - R \cdot \phi_{\text{geo}}^{\text{low}}) + (\phi_{\text{tro}}^{\text{high}} - R \cdot \phi_{\text{tro}}^{\text{low}}) \\ & + (\phi_{\text{ion}}^{\text{high}} - R \cdot \phi_{\text{ion}}^{\text{low}}) + (\phi_{\text{inst}}^{\text{high}} - R \cdot \phi_{\text{inst}}^{\text{low}}) \\ & + 2\pi(n^{\text{high}} - R \cdot n^{\text{low}}), \end{aligned} \quad (1)$$

where $\phi_{\text{geo}}^{\text{low}}, \phi_{\text{tro}}^{\text{low}}, \phi_{\text{ion}}^{\text{low}}, \phi_{\text{inst}}^{\text{low}}, \phi_{\text{geo}}^{\text{high}}, \phi_{\text{tro}}^{\text{high}}, \phi_{\text{ion}}^{\text{high}}$ and $\phi_{\text{inst}}^{\text{high}}$ are the contributions arising from geometric, tropospheric, ionospheric and instrumental inadequacies in the delay model for, respectively, either the low or high frequency. n^{low} and n^{high} are the integer number of full phase rotations, or ambiguities in the phase, for each of the frequencies and R is the frequency ratio between the high and low frequencies. At mm-wavelengths the geometric and tropospheric phase residual terms will scale with frequency and therefore these terms in parenthesis will cancel; instrumental terms are assumed to have been dealt with using observations of a primary calibrator. Whereas the ionospheric terms, although non-zero, are slow-changing in time and equal over a large angular separation. When R is an integer the phases from the ambiguity terms n are always integer multiples of 2π , so are not relevant to the analysis. However when R is not an integer phase jumps are introduced every time n^{low} changes. That is at every introduction of an ambiguity in phase there will be a step in the

phase of ϕ^{FPT} , which can not be corrected from the observations of the second source, as for the calibrator the number of ambiguities is independent along that different line of sight. Clearly the solution for non-integer frequency ratio SFPR is equivalent to that required to avoid introducing any untracked lobe rotations in the visibility data. Below we describe our data reduction procedure to retain the astrometric information, even when the ratio between the observing frequencies is not an integer number.

3.2. Source Frequency Phase Referencing with non-integer frequency ratios

We used the NRAO AIPS software package for the data reduction (Griesen 2003). The information on measured system temperatures, telescope gains, and estimated bandpass corrections for the individual antennae were used to calibrate the raw correlation coefficients of the continuum calibrators and of the target spectral line source. Figure 2 shows a schematic of the steps after this initial calibration for each source and for each frequency, indicating the transfer of the calibration tables. Each of the four columns in that figure represents a different stage in the analysis.

Column 1 is for the reference source at the reference frequency, i.e. 4C39.25 at 22 GHz. The first step is to use the AIPS task FRING, which is a global self-calibration algorithm (Cotton 1995), to estimate residual antenna-based VLBI phases, and its partial derivatives, with respect to frequency (group delay, τ), and time (phase delay rate), on the calibrator (4C39.25) data set. These terms result from unaccounted contributions from the atmospheric propagation and from errors in the array geometry during the data correlation. The performance of the digital filters in the KVN optics (Han et al. 2013) and backend (Oh et al. 2011) is extremely good, particularly in the absence of instrumental phase offsets introduced by the electronics at each IF and band. This enables the straight-forward use of all the IFs as an effective single bandwidth for the estimation of a more precise group delay (since $\sigma_\tau \propto 1/\text{bandwidth}$) (Schwab & Cotton 1983). With a reasonable SNR and 432MHz spanned bandwidth we expect delay accuracies of tens of picoseconds. We used the delays derived from this calibrator and frequency, solving for a single delay across all the IFs, in all the subsequent analysis of the other sources and frequencies. Finally for this source and frequency we applied the small ($<10^\circ$) phase corrections which were constant across the whole experiment, to align the IFs. These were derived with the phase self-calibration task CALIB; normally this would be done with FRING on a single scan of a strong calibrator but we applied this as a refinement after the application of the initial calibration across all the observations as the single band delay corrections required for the KVN receiver were essentially zero.

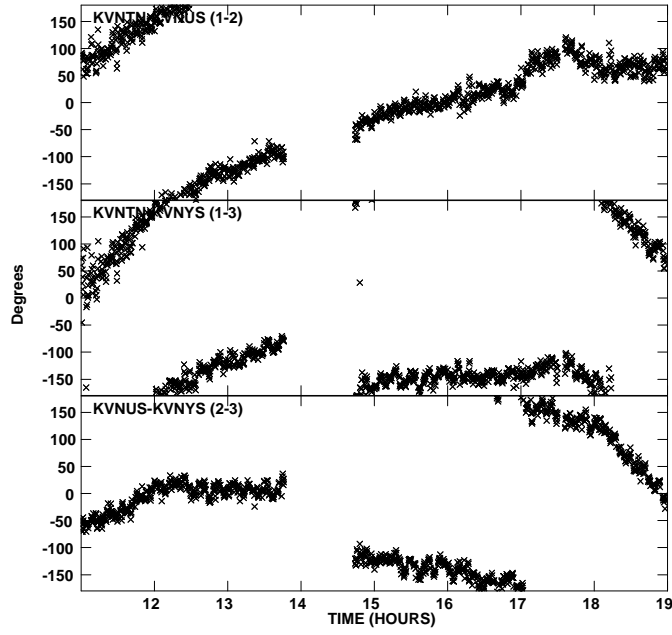


Fig. 1.— Residual visibility phases of 4C39.25 at 43GHz after the Frequency Phase Transfer step, that is the application of the scaled corrections derived at 22GHz on the simultaneous low frequency observations. Whilst the phases are disciplined and have coherence timescales of the order of an hour, the remaining dispersive terms prevent direct imaging.

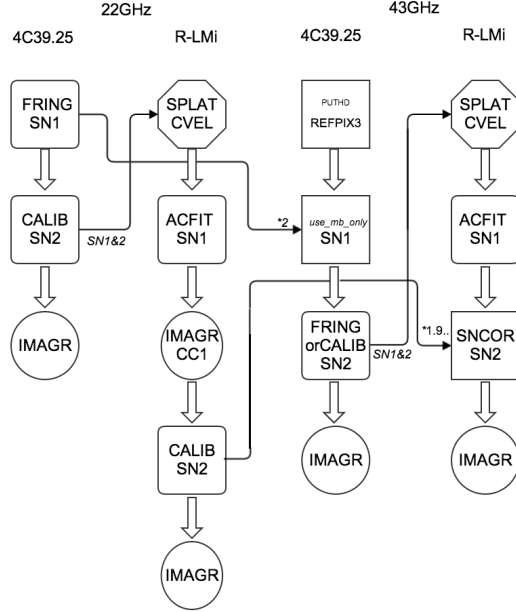


Fig. 2.— Schematic flow for the non-integer SFPR data reduction. ‘Rounded squares’ (e.g. FRING or CALIB) are calibration derivations, ‘Squares’ are operations on those calibration values. ‘Hexagons’ are operations on the uv -data and circles are the ‘inversion’ of the uv -data to form the image. In all cases the AIPS task and the calibration table are specified.

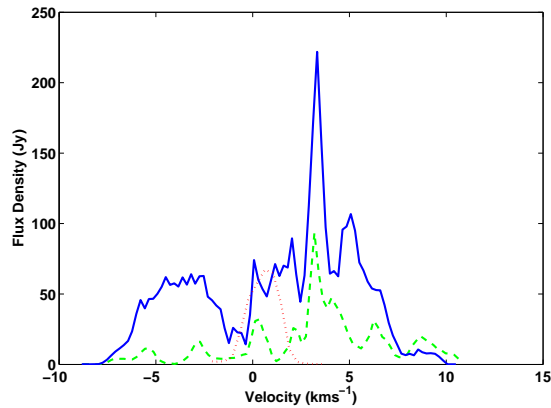


Fig. 3.— Maser Spectra for H₂O (red dotted line) and SiO $v=2$ (green dashed line) and $v=1$ (blue solid line) determined from the sum of the model components fitted to the image cube.

With these calibration steps completed we (Column 2, Fig. 2) calibrated and separated the IF with the spectral line RLMi H₂O maser data and applied the doppler corrections using the LSR standard of rest and Radio velocity definitions (with SPLAT and CVEL) (Reid 1995). Additional corrections to the amplitudes could be derived with ACFIT at this point; these were the order of 10% and are possibly from the uncorrected atmospheric opacity. The 22GHz phase referenced spectral line data could then be imaged and a channel with a compact, strong, point source dominated emission was selected for further analysis. It was immediately obvious where the peak of the brightness fell in the image and a single model component at the site of this peak was used for a phase refinement of the data, generated by CALIB, followed by re-imaging and deconvolution. This latter step, which is mainly correcting for the differential static atmospheric contributions, would lose the astrometrical registration if we were not able to find a reasonable apriori position for the conventionally phase referenced data and use that for the calibration model. Therefore one of the requirements for successful non-integer SFPR is that an adequate initial phase referenced image can be formed. As the accuracy we require for this position is a few mas this is not an overly demanding requirement. The outcome is that the first step produces a conventional PR image of the H₂O masers, and the second provides phase refinements to that dataset whilst retaining the location of the maximum emission. Therefore the H₂O maser cube is registered to the 4C39.25 calibrator. Figure 3 plots the spectra of the recovered emission (i.e. the flux density in the clean components) from the H₂O image cube with a red dotted line.

The 43GHz 4C39.25 data (Column 3, Fig. 2) was first adjusted so that the reference frequency value was set, using AIPS task PUTHEAD, to 43.620 GHz; that is double the reference frequency value of the lower frequency and outside the observed band. The frequency axis reference pixel was also changed. This ensured the labelling of the data was correct while preserving an integer reference frequency ratio and the phases could be doubled without considerations of the ambiguities. These two steps are specifically required for non-integer frequency ratio analysis. Then we doubled the value of phases measured from the delay observations of 4C39.25 at 22 GHz, using our own external script, to produce a FPT dataset. As a word of warning to users we mention that we do not recommend the AIPS task SNCOR for this purpose, as it does not do a good job when there are multiple IFs unless the separations between the IFs also scale by the same frequency ratio factor. However, it functions correctly when there is only one IF per frequency band. We calibrated the remaining dispersive phase corrections, which were changing on \sim hour long timescales, with CALIB.

Once again (Column 4, Fig. 2) we calibrated and separated those IFs with the RLMi SiO maser data using SPLAT, using the scaled 4C39.25 delays from 22GHz and the dispersive

phase corrections from 4C39.25 at 43GHz. The doppler and amplitude corrections were calculated with CVEL and ACFIT as before. We transferred the phase solutions from the H₂O maser and scaled these values by the frequency ratio between the H₂O and the SiO maser $v=1$ and $v=2$, that is 1.939 and 1.926 respectively. This data was then ready for imaging. However the images were not of very good quality and looking back at the solutions it was clear that in the observing gap at zenith, a turn of phase had been missed on the Ulsan antenna in the second half of the experiment. We added in the phase jump that would have been introduced by this missed turn of phase ($2\pi(2 - \nu_{\text{SiO}}/\nu_{\text{H}_2\text{O}})$ for the two transitions, equal to 27° and 22° respectively) using SNCOR. Figure 4 shows the measured phase corrections (i.e. the phase residuals) for the H₂O maser and the derived corrections for the SiO $v=1$ maser before and after adding in the lost phase turn. With these steps completed we were able to directly image the SiO masers at the two transitions, which were now accurately registered to the H₂O emission and that in turn to 4C39.25. We imaged the data via the normal methods. Given the limited number of baselines we found the most reliable deconvolution came with fitting a small number of model components to the data, which we did in difmap (Shepherd et al. 1994). Figure 3 plots with a blue and green solid and dashed lines the spectra of the recovered emission (i.e. the flux density in the clean components) from the SiO image cubes. The images are shown in Section 4. Plotting of the cubes for the figures in this paper was done with Miriad (Sault et al. 1995).

4. Results

4.1. Astrometric Imaging

Our analysis followed the steps required to produce PR maps of the H₂O maser emission, with respect to 4C39.25 and SFPR maps of the two transitions of SiO maser emission, with respect to the H₂O maser emission. We present images of the astrometrically registered velocity averaged (moment zero) cubes of the H₂O and SiO maser emission (Figure 5) and astrometrically registered velocity cubes of the two transitions of SiO maser emission (Figure 6). The image coordinates are relative to the peak of the SiO maser emission in $v=1$. On Figure 5 we have overlaid the position of the optical source R LMi, as measured by Hipparcos, for the observing epoch (2011.17) with 1σ errors (shown with a large cross) (van Leeuwen 2007). This position is listed in Table 1, which summarises all the astrometric positions we have measured. The Hipparcos position has errors that are dominated by the measurement errors in the proper motion, multiplied by the two decades since those observations were made. We measured the peak of the H₂O emission with IMFIT in the moment zero map, which is listed in Table 1 with the formal errors on that fit. The much larger systematic

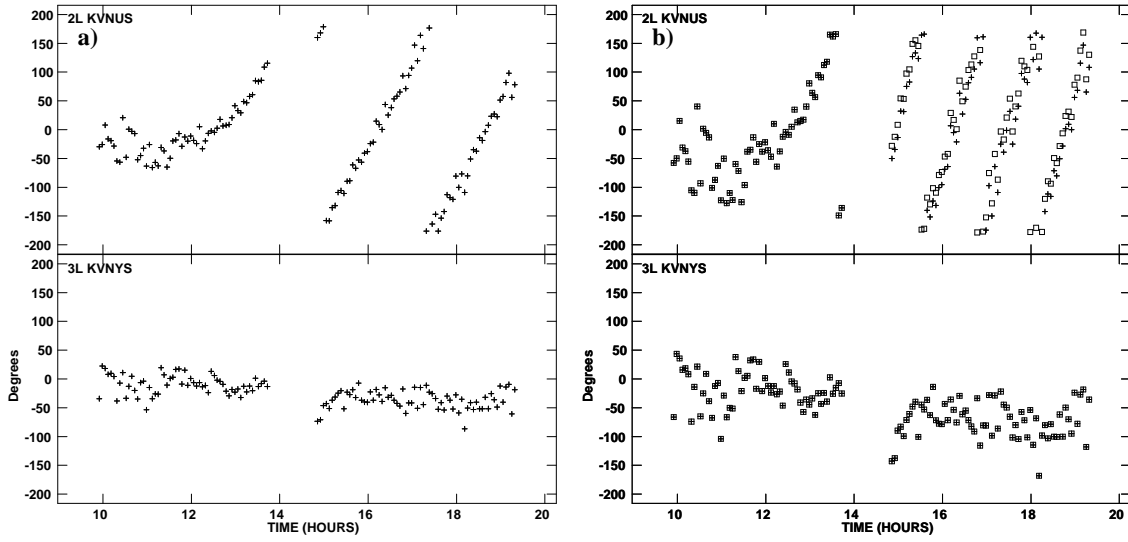


Fig. 4.— Plots of a) the antenna-based phase-residual corrections to the FPT data, on the H_2O maser observed at 22GHz, derived by self-calibration with CALIB and b) the corrections derived for the $\text{SiO } v=1$ maser by scaling with the non-integer frequency ratio between the two transitions both before correcting for the dropped turn of phase at zenith (crosses) and after correcting for the dropped turn of phase (squares). The shift between the two solutions is 22° .

errors are discussed in the following section. Similarly the peak of the SiO $v=1$ emission was measured and the position and errors are in the same table. We fitted a ring to a mask of the combined $v=1$ and 2 emission, by a least-square maximisation of the overlap of a ring model with the pixels in the image in either transition with emission greater than 10% of the peak in that transition. The centre of this ring should be the site of the centre of optical emission of RLMi. We take the width of the ring as the uncertainty in that position. The ring is shown as the circle, with the centre and the uncertainty shown with a small cross, in both Figures 5 and 6. The values are listed in Table 1.

4.2. Error Analysis

The errors in Table 1 are the formal errors in the fitting to the data. For the VLBI data these are completely dominated by the systematic effects, which we review here.

The H₂O maser peak emission position is conventionally phase referenced to 4C39.25, which has a very accurate absolute reference position with errors of about 0.1mas (Fey et al. 2004), but an angular separation of 5.9° from the RLMi target. Because of this large separation this would not normally be considered a good phase referencing calibrator. With such an observing setup, even in good weather, one would expect of the order of 30° of phase noise from the dynamic tropospheric contributions, more than 100° of phase noise from the static tropospheric contributions, 15° of phase noise from the static ionospheric contributions and less than 1° of phase noise from the dynamic ionospheric contributions (following the formulae in Asaki et al. (2007)). However we note that the atmospheric coherence of the KVN appears to be much better than those for the typical cases (Lee et al. 2014). This maybe due to better coherence between the atmosphere at the different sites, which could be from the short baselines or that the weather moves down off the Chinese landmass with little disruption. Various methods exist to reduce the dominant static tropospheric contributions, as reviewed in Honma et al. (2008), but these were not followed in this experimental setup as we did not originally intend to attempt to achieve absolute astrometric connection. Nevertheless on inspection of the data we realised that should be possible, as the peak of the brightness was clearly identifiable. To confirm that errors were minor we compared the peak flux before and after self calibration. This gives a measure of the scale of the random errors. If these errors are small one can be confident that the data is largely coherent and the astrometry is preserved. The fractional flux recovery we found for the whole data set was 86%, and 96% for the data taken in the first half of the experiment. For our analysis we took the position of the water maser peak from a model fit of a single component to the data, limited to regions where the phase residuals were smallest. That is the data between

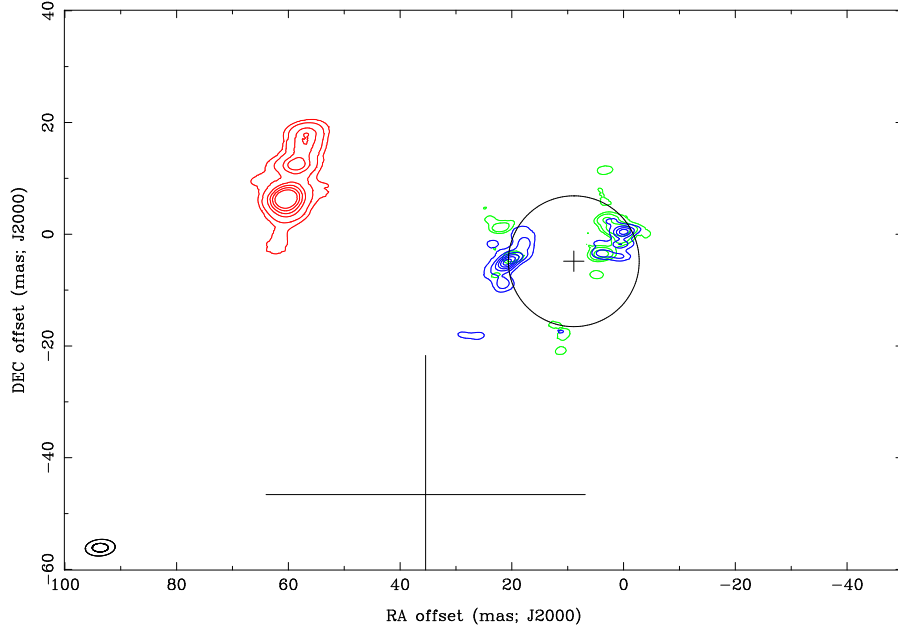


Fig. 5.— Contour plots of the Moment Zero integrated SFPR maps with absolute astrometry relative to the peak of the SiO $v=1$, $J=0 \rightarrow 1$ emission centred at 09:45:34.284 +34:30:42.765 (epoch 2011.7 in equinox J2000 coordinates). The $v=1$ SiO emission (in blue) has contour levels of 10 to 80 Jy/bm km s $^{-1}$ in steps of 10, and the $v=2$ (green) has contour levels of 3 to 24 Jy/bm km s $^{-1}$ doubling at every step. The H $_2$ O maser emission (red) is overlaid with contour levels of 3, 6, 12, 16 20 & 24 Jy/bm km s $^{-1}$. The boundary and the centre of the ring fitted to the SiO emission, and the uncertainties in the fitting, is included as the circle with small cross at centre. This would be expected to centre on the R Leo Minoris optical emission. The large cross indicates the Hipparcos position for this source, with the bar length being the proper motion error over the 21 years since the optical positional epoch. The beam for the two bands appears in the bottom left.

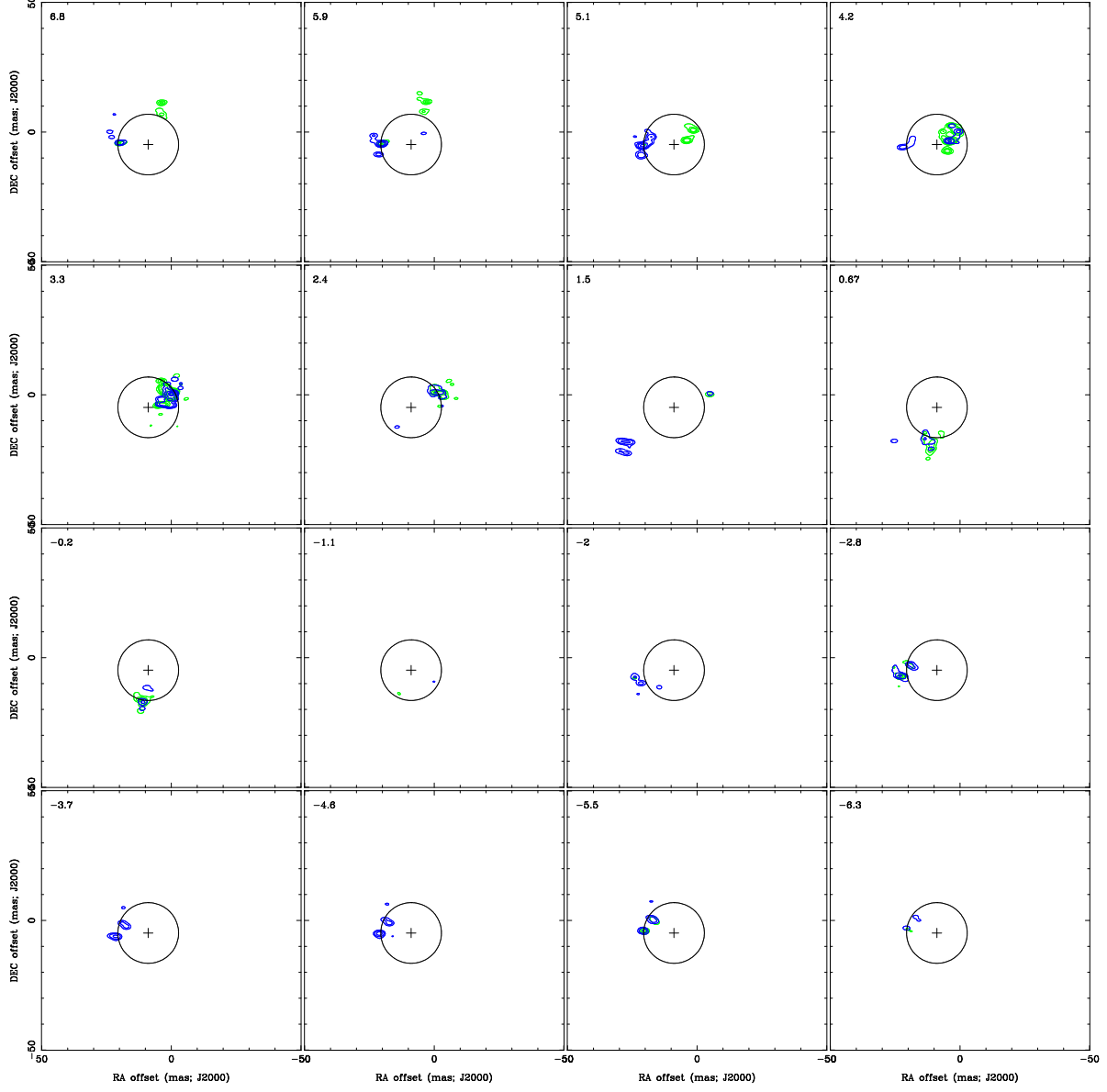


Fig. 6.— Contour plot of the Velocity Channels map of the SiO emission in $v=1$ (blue) and $v=2$ (green) for $J=0 \rightarrow 1$ centred on the peak emission. The circle for the SiO emission from Figure 5 is included. The data are averaged to 0.9 km s^{-1} channels with contours at 1, 2, 3, 6, 12, 24 and 32 Jy km s^{-1} for $v=2$ and at 3, 6, 12, 24 and 50 Jy kms for $v=1$. The average velocity is given in the top left of each panel.

Yonsei and Tamna, plus Ulsan in the first half of the experiment, which had a fractional flux recovery of 91%. Given the large angular separation between the sources we take a generous upper bound for the positional errors to be the resolution, 5×3 mas. In future work we will attempt to improve on these limits.

The optical star RLMi has a relatively poor a priori position from Hipparcos. The uncertainty is in the proper motion measurement which, given that the Hipparcos data is referenced to the observational epoch of 1991.25, results in a position error of ~ 50 mas. However as we phase reference the H_2O maser emission to 4C39.25 the positional errors in our analysis are less. Taking this as the dominant source of error in our analysis we use it to determine the final error bars in our astrometric measurements between the maser transitions. We use the relationship of $\Delta\nu/\nu \cdot \Delta\theta$, where $\Delta\theta$ is the astrometric accuracy of the reference (i.e. the H_2O emission) and $\Delta\nu$ is the frequency gap between the transitions. In this case the registration would, with $\Delta\theta$ of 5 mas, have an uncertainty of 2.5 mas between the H_2O and the SiO and $35 \mu\text{as}$ between the SiO $v=1$ and 2 masers. In both cases the typical separations between, firstly the H_2O and the SiO masers and the second case between the SiO $v=1$ and 2 masers, are much greater than these errors, which will allow us to have faith in any separations detected. SiO rings are close to the surface of the star and water masers maybe ten times further out (10^{15}cm), which implies a typical separation of 60 mas between the sites of the H_2O and the SiO maser emission for a source at 1 kpc; that is the astrometric errors would be the order of 4%. An error in astrometry of $35 \mu\text{as}$ between the SiO maser transitions implies a physical scale of $5 \times 10^{11}\text{cm}$ at 1 kpc, or 0.5% of the typical ring diameter (10^{14}cm).

The retention of absolute astrometric registration in the VLBI data allows us to compare the centre of the SiO maser emission, where the star in RLMi should be, and the Hipparcos position for this star. Measuring from the astrometric image derived, we find the position offset between these to be -33 and 41 mas. The error budget on this measurement consists of the errors in the fit to the centre of the circle, which is 5 mas, combined with the absolute astrometric accuracy of the H_2O emission gives a total estimated error of 7 mas. Given the twenty years since the Hipparcos reference epoch the errors in proper motion from the Hipparcos data dominate. The centre of the circle of SiO maser emission falls within the 1σ error ($\sigma_{\text{RA}_{\text{pm}}} = 35$ mas) in the Hipparcos value of along $\mu_{\text{acos}\delta}$ and within the 2σ error ($\sigma_{\delta_{\text{pm}}} = 25$ mas) in the Hipparcos value of along μ_{δ} (van Leeuwen 2007). Forthcoming observations from the GAIA satellite (Perryman et al. 2001) will be able to confirm this VLBI result.

Combining the VLBI position we have derived in 2011.17, with uncertainties in the fit and those of the H_2O maser emission to give a total of 7 mas, with that of Hipparcos from 1991.25, with uncertainties of 1 mas, we can derive the proper motion of RLMi over the

twenty year baseline and this is given in Table 1.

Subtracted from (both) the reported VLBI positions would be the core shift (and any other structure phases) from 4C39.25 which, because it was assumed to be achromatic in the analysis, would contaminate these results. These effects are far below the levels of accuracy achieved in this analysis but will become significant when global baselines are included.

5. Discussion

We report here astrometrically aligned images of the H₂O and SiO masers around R LMi. This is the first demonstration of the SFPR method with non-integer frequency phase ratios, and the first demonstration of the combination of SFPR with PR to retain absolute astrometry through out the analytical chain. Our error analysis cautiously sets large errors on the absolute position of the H₂O maser emission, and these errors are matched by the uncertainty in the ring fitting to find the centre of the SiO maser emission, but these are still a major improvement in the uncertainty in the Hipparcos position for this source.

There have been previous attempts to make astrometrical observations for AGB stars with SiO and H₂O masers. A limited number were made with VERA and so provide bonafide astrometry, the others do not. Now, with the new methods discussed here, mm-VLBI astrometric line experiments will become much more straight forward and, we hope, widely implemented. We will, now the method is understood, undertake a major monitoring campaign of interesting AGBs hosting H₂O and SiO masers, and massive star forming regions hosting H₂O and CH₃OH masers – potentially up to and including the 95GHz line. To aid other users who wish to follow the same analysis we provide a list of what we consider the required conditions for a successful outcome.

5.1. Crucial considerations for success

- SFPR requires that the calibrator is within the same ionospheric region (the ‘patch’) for dispersive contributions. Fortunately the patch size scales with frequency so for high frequencies this will be very large. The actual scale size at mm-frequencies is under investigation; extrapolating from measurements at lower frequencies (e.g. Thompson et al. (2001)) is not possible as the approximations are no longer valid. In Rioja & Dodson (2011) we have successfully used calibrators 10° from the target.
- SFPR for spectral-line sources must use the delays derived from the continuum calibrator source, as the line of sight corrections to the delays are not derivable on the line

source. Therefore the antenna position errors must be sufficiently small (less than a few cm) so that they do not introduce rapid phase changes which could not be tracked on the other source.

- Non-integer frequency ratio SFPR requires the delay solutions to be of sufficient quality to allow extrapolation to a reference point outside of the observing band. A 0.05 nsec error in the delay would introduce a 9° error in the phase for a point 500MHz from the frequency reference pixel. We suggest that one should try and ensure this extrapolation is no further than the bandwidth spanned.
- Non-integer frequency ratio SFPR requires that the phase solutions can be tracked across wraps of phase ambiguities, so continuous observations without gaps are desirable.
- Non-integer frequency ratio SFPR also requires that the positions of the target source at the lower frequency are accurate. The absolute error in the target position at the reference frequency, when applied to the target frequency, is diluted by the fractional frequency span $\Delta\nu/\nu$. For SFPR this fractional span approaches integer so that the errors in the registration between the frequencies can approach the absolute positional error. If needed the positions can be derived by conventionally phase referencing the low frequency data. In this case the source switching needs to be sufficiently fast to allow phase referencing at the low frequency.
- For arrays which don't support (yet) simultaneous multichannel receivers (e.g. the VLBA) fast frequency switching will still work with this approach. Fast frequency switching is limited in the maximum frequencies which can be supported (as the variation in the rates can not be higher than the cycle time of the frequency switching). In our experience fast frequency switching between frequencies as high as 43 and 86 GHz is achievable in good conditions with switching cycle period of 1 minute. This is about the maximum speed possible with the VLBA sub-reflector rotator.

6. Conclusions

We have demonstrated that the KVN is capable of performing non-integer Source Frequency Phase Referencing on simultaneously observed line sources, between H₂O and SiO in this particular case. The method would also be suitable for H₂O and 44GHz CH₃OH targets. This would provide astrometric positions between all the transitions, and potentially (if the H₂O masers are phase referenced) absolute astrometric positions for all the transitions, as in this case.

Our method allows a high quality mas-level astrometric alignment of the two SiO frequencies with respect to the H₂O emission. The registration to 4C39.25 and the absolute coordinate system is based on how far one trusts the conventional phase referencing. We have explained why we believe that the errors in the H₂O maser position are less than 5 mas. This provides a much improved position for the centre of a ring containing the SiO emission, which would be the site of the optical source. This position is within the errors from the Hipparcos observations. The error on the fit to the centre of the circle is 5 mas, which when combined with the absolute astrometric accuracy of the H₂O emission gives a total estimated error of 7 mas. From the new position we are able to improve on the proper motion derived by Hipparcos for the optical star R LMi, improving the precision by nearly an order of magnitude, to 0.3 mas/yr.

The registration between the two SiO transitions is expected to be the order of 35 μ as, which will allow for very exact separation of the location of the different masing components. The registration of the H₂O and the SiO maser emission has an error of 2.5 mas. Detailed analysis of the SiO emission structure is left for future publications, when we have monitored the SiO masers through the full cycle of the pulsation period. Additionally in the near future we are hopeful of being able to access longer baselines to Japan, Spain or Australia, which would provide a desirable boost in resolution.

Acknowledgements

We are grateful to all staff members and students in the KVN who helped to operate the array. The KVN is a facility operated by the Korea Astronomy and Space Science Institute. RD acknowledges the support of the Korean Ministry of Science, ICT & Future Planning Brainpool Fellowship (121S-1-2-0228). We acknowledge with thanks the variable star observations from the AAVSO International Database, contributed by observers worldwide, that provided the optical phase for our observations. We wish to thank the anonymous referee, whose comments improved the presentation of the material in this paper.

REFERENCES

- Alef, W. 1988, The Impact of VLBI on Astrophysics and Geophysics, 129, 523
- Asaki, Y., Sudou, H., Kono, Y., et al. 2007, PASJ, 59, 397
- Beasley, A. J., & Conway, J. E. 1995, Very Long Baseline Interferometry and the VLBA, 82, 327
- Benson, P. J., & Little-Marenin, I. R. 1996, ApJS, 106, 579

- Boboltz, D. A., & Wittkowski, M. 2005, *ApJ*, 618, 953
- Bowen, G. H. 1988, *ApJ*, 329, 299
- Bujarrabal, V. 1994, *A&A*, 285, 971
- Choi Y. K., Hirota T., Honma M., Kobayashi H., Proceedings of the 9th European VLBI Network Symposium, “Distance to VY Canis Majoris with VERA”. SISSA, Trieste; 2008.
- Cooke, B., & Elitzur, M. 1985, *ApJ*, 295, 175
- Cotton, W. D., Ragland, S., & Danchi, W. C. 2011, *ApJ*, 736, 96
- Cotton, W. D., Ragland, S., Pluzhnik, E. A., et al. 2010, *ApJS*, 188, 506
- Cotton, W. D., Ragland, S., Pluzhnik, E. A., et al. 2010, *ApJS*, 187, 107
- Cotton, W. D., Ragland, S., Pluzhnik, E. A., et al. 2009, *ApJS*, 185, 574
- Cotton, W. D., Ragland, S., Pluzhnik, E., et al. 2009, *ApJ*, 704, 170
- Cotton, W. D., Perrin, G., & Lopez, B. 2008, *A&A*, 477, 853
- Cotton, W. D., et al. 2006, *A&A*, 456, 339
- Cotton, W. D., et al. 2004, *A&A*, 414, 275
- Cotton, W. D. 1995, *Very Long Baseline Interferometry and the VLBA*, 82, 189
- Desmurs, J. F., Bujarrabal, V., Colomer, F., & Alcolea, J. 2000, *A&A*, 360, 189
- Deller, A. T., Brisken, W. F., Phillips, C. J., et al. 2011, *PASP*, 123, 275
- Dodson, R., & Rioja, M. J. 2009, *VLBA Science Memo #31*
- Dodson, R., Rioja, M. J., Jung T.H., 2011, *East Asia VLBI Workshop*, Lijiang, China.
- Elitzur, M. 1980, *ApJ*, 240, 553
- Elitzur, M. 1992, *ARA&A*, 30, 75
- Fey, A.L., et al., 2004, *AJ*, 127, 3587
- Fomalont, E., 2014, *Personal Comms*.

- Han, S.-T., Lee, J.-W., Kang, J., et al. 2008, *International Journal of Infrared and Millimeter Waves*, 29, 69
- Han, S.-T., Lee, J.-W., Kang, J., et al. 2013, *PASP*, 125, 539
- Honma, M., Tamura, Y., & Reid, M. J. 2008, *PASJ*, 60, 951
- Humphreys, E. M. L., Gray, M. D., Yates, J. A., Field, D., Bowen, G., & Diamond, P. J. 2000, *EVN Symposium 2000, Proceedings of the 5th european VLBI Network Symposium*, 197
- Humphreys, E.M.L., Gray, M.D., Yates, J.A., et al. 2002, *A&A*, 385, 256
- Gray, M. D., Humphreys, E. M. L., & Yates, J. A. 1999, *MNRAS*, 304, 906
- Gray, M. D., Wittkowski, M., Scholz, M., et al. 2009, *MNRAS*, 394, 51
- Griesen, E. W., 2003, in *Information Handling in Astronomy – Historical Vistas*, Heck, A. ed., Kluwer Academic Publishers, Dordrecht, ISBN 1-4040-1178-4, *Astrophysics and Space Science Library*, 285, 109.
- Lee, S.-S., et al. 2014, *AJ*, 147, 77
- Kamohara, R., Bujarrabal, V., Honma, M., et al. 2010, *A&A*, 510, A69
- Keenan P.C., Garrison, R.F., Deutsch, A.J., 1974, *ApJS*, 28, 271
- Kim, J., Cho, S.-H., Oh, C. S., & Byun, D.-Y. 2010, *ApJS*, 188, 209
- Oh, S.-J., et al., 2011, *Publications of the Astronomical Society of Japan*, 63, 1229
- Pardo, J. R., Alcolea, J., Bujarrabal, V., Colomer, F., del Romero, A., & de Vicente, P. 2004, *A&A*, 424, 145
- Perryman, M.A.C., et al. 1997, *A&A*, 323, L49
- Perryman, M. A. C., de Boer, K. S., Gilmore, G., et al. 2001, *A&A*, 369, 339
- Pickles, A. & Depagne, É., 2010, *PASP*, 122, 1437
- Reid, M. J. 1995, *Very Long Baseline Interferometry and the VLBA*, 82, 209
- Richter, L., Kembell, A., & Jonas, J. 2013, *MNRAS*, 436, 1708
- Rioja, M., Dodson, R., Malarecki, J., & Asaki, Y. 2011, *AJ*, 142, 157

- Rioja, M., & Dodson, R. 2011, *AJ*, 141, 114
- Rioja, M. J., & Dodson, R. 2009, VLBA Science Memo #32
- Rioja, M. J., Dodson, R., Kamohara, R., et al. 2008, *PASJ*, 60, 1031
- Rioja, M. J., Dodson, R., et al. 2014, Manuscript AJ-12041
- Schwab, F. R., & Cotton, W. D. 1983, *AJ*, 88, 688
- Shepherd, M. C., Pearson, T. J., & Taylor, G. B. 1994, *BAAS*, 26, 987
- Soria-Ruiz, R., Alcolea, J., Colomer, F., Bujarrabal, V., Desmurs, J.-F., Marvel, K. B., & Diamond, P. J. 2004, *A&A*, 426, 131
- Soria-Ruiz, R., Colomer, F., Alcolea, J., Bujarrabal, V., Desmurs, J.-F., & Marvel, K. B. 2005, *A&A*, 432, L39
- Soria-Ruiz, R., Alcolea, J., Colomer, F., Bujarrabal, V., & Desmurs, J.-F. 2007, *A&A*, 468, L1
- Sault, R. J., Teuben, P. J., & Wright, M. C. H. 1995, *Astronomical Data Analysis Software and Systems IV*, 77, 433
- Thompson, A. R., Moran, J. M., & Swenson, G. W., Jr. 2001, "Interferometry and synthesis in radio astronomy by A. Richard Thompson, James M. Moran, and George W. Swenson, Jr. 2nd ed. New York : Wiley
- van Leeuwen, F. 2007, *Astrophysics and Space Science Library*, 350,
- Whitelock, P., Feast, M., & van Leeuwen, F. 2008, *MNRAS*, 386, 313
- Yi, J., Booth, R.S., Conway, J.E., Diamond, P.J., 2005, *A&A*, 432, 531

Astrometric Positions of Sources at Epoch 2011.17

	α_{2000} h:m:s	$\Delta\alpha$ mas	δ_{2000} d:m:s	$\Delta\delta$ mas
Predicted Hipparcos position of R LMi	09:45:34.2867	42	+34:30:42.718	25
Peak of H ₂ O maser emission	09:45:34.2890	0.6	+34:30:42.771	0.4
Peak of the SiO $v=1$ emission	09:45:34.2838	0.4	+34:30:42.765	0.4
Centre of SiO emission ($v=2$ and 1)	09:45:34.2845	5	+34:30:42.759	5

Implied Proper Motion of R LMi

	$\mu_{\alpha\cos\delta}$ mas/yr	$\Delta\mu_{\alpha\cos\delta}$ mas/yr	μ_{δ} mas/yr	$\Delta\mu_{\delta}$ mas/yr
Combined Hipparcos and VLBI observations	2.3	0.3	-3.9	0.3

Table 1: Astrometric Positions of R LMi for optical, H₂O and SiO emission for epoch 2011.17, with formal 1- σ errors. Assuming the Hipparcos position of epoch 1991.25 and the centroid of the SiO of epoch 2011.17 are compatible provides an improved proper motion value.

This figure "fig2.png" is available in "png" format from:

<http://arxiv.org/ps/1408.3513v1>